

Flexible Physical Camouflage Generation Based on a Differential Approach

Yang Li^{1*}, Wenyi Tan¹, Chenxing Zhao¹, Shuangju Zhou¹, Xinkai Liang², and Quan Pan¹

¹School of Automation, Northwestern Polytechnical University, Xi'an, China

²Laboratory of Science and Technology on Complex System Control and Intelligent Agent Cooperation, Beijing, China

Abstract

This study introduces a novel approach to neural rendering, specifically tailored for adversarial camouflage, within an extensive 3D rendering framework. Our method, named FPA, goes beyond traditional techniques by faithfully simulating lighting conditions and material variations, ensuring a nuanced and realistic representation of textures on a 3D target. To achieve this, we employ a generative approach that learns adversarial patterns from a diffusion model. This involves incorporating a specially designed adversarial loss and covert constraint loss to guarantee the adversarial and covert nature of the camouflage in the physical world. Furthermore, we showcase the effectiveness of the proposed camouflage in sticker mode, demonstrating its ability to cover the target without compromising adversarial information. Through empirical and physical experiments, FPA exhibits strong performance in terms of attack success rate and transferability. Additionally, the designed sticker-mode camouflage, coupled with a concealment constraint, adapts to the environment, yielding diverse styles of texture. Our findings highlight the versatility and efficacy of the FPA approach in adversarial camouflage applications.

1 Introduction

Previous research has validated the vulnerability of the neural network. Especially in the work of computer vision [27, 61], natural language processing [28], and deep reinforcement learning [25, 26]. While most of them conduct the attack in the digital space, tasks e.g., facial recognition [55, 60], image classification [35, 36], etc., by crafting specially designed perturbation, adversarial patches, etc. Though the patch can be printed out to deploy the physical attack, environmental factors such as view angle, light, hue, etc., deeply affect the attack. Therefore, it is more difficult to conduct an adversarial attack on the model in the physical world as the complex physical constraints (camera pose, etc.).

Recently, the camouflage attack has sprung out by optimizing the adversarial pattern which can be attached to the entire

body of the target (e.g., individuals, vehicles, etc.). Different from the patched attack, the camouflage attack needs to take care of an all-round attack and non-rigid structures on the target surface. Therefore, the two most critical aspects of a camouflage attack involve the method of texture generation and the rendering technology applied to the target surface. According to existing works, there are primarily two methods for texture generation: One approach is based on optimizing texture images, achieving full vehicle camouflage through repeated texture overlays [53, 57]. However, such camouflage struggles to effectively deceive target detectors when facing different distances and viewing angles. The other method involves optimizing the entire area of the target surface that requires texture coverage as a whole [47, 48]. Each part of the texture corresponds to a specific region on the target surface, providing better robustness against changes in viewpoint and occlusion. However, this approach increases the size of the texture, resulting in longer rendering times and making optimization more challenging. Another challenge in camouflage attacks is the rendering of textures onto the target surface. Because 3D targets are non-planar, simulating the coverage status in real-world environments becomes more difficult. To address this issue, some works use neural rendering to map textures [47], but they cannot simulate physical factors' interference. Another line of work, such as DTA [41] and ACTIVE [42], designs differentiable neural renderers that can learn various scene attributes, enabling the generation of adversarial camouflage in a black-box manner. However, it's worth noting that neural renderers demand extensive data for learning rendering, requiring substantial labeled data. Furthermore, the training data cannot be changed dynamically during the training process, leading to a lack of inherent generalization in the generated texture. In all the aforementioned works, the camouflage covering the target surface cannot be unfolded in UV maps. Consequently, additional processing of textures is required before physical deployment, which increases the risk of adversarial information loss, extends actual deployment time, and lacks flexibility.

In response to the aforementioned challenges and in pursuit

of an approach that allows for an adversarial in a sticker manner, enabling the selection of specific areas to cover with adversarial camouflage, we introduce a novel framework, termed Flexible Physical-camouflage Attack (FPA). Diverging from traditional neural rendering approaches, we fashioned a renderer for adversarial camouflage by leveraging a differentiable mesh renderer framework. Within this framework, we harnessed modular differentiable rendering functions to simulate authentic lighting conditions and material variations, ensuring a nuanced representation of the 3D target’s textures. This approach took into account variables such as lighting and material properties, contributing to a more realistic rendering outcome. Then, we learn the adversarial pattern from the diffusion model in a generative way and combine the designed adversarial loss and covert constraint loss to guarantee the adversarial camouflage’s adversarial and covert nature in the physical world. Meanwhile, the camouflage in sticker mode can easily cover the target in the physical world without losing too much adversarial information. The contribution of this work can be summarized as follows:

- We established a rendering system rooted in a robust 3D framework, sidestepping the intricacies associated with training neural renderers and achieving heightened rendering efficiency. Meanwhile, in combination with the Blender tool, it can generate adversarial camouflage in the form of stickers, minimizing the loss of adversarial information for physical deployment and enhancing the flexibility for application in the physical world.
- We learn adversarial patterns from diffusion models, and the learned adversarial patterns are more realistic. This approach enables us to expedite the optimization process when generating higher-resolution adversarial camouflage while ensuring clearer camouflage textures.
- We introduce novel confrontation loss and concealment constraint loss, which effectively enhance the aggressiveness and concealment of camouflage, facilitating adaptation to diverse environments.

2 Related Works

Given the prevalent utilization of adversarial samples, there has been a notable shift in research focus towards physical-world attacks, predominantly manifesting as adversarial patches and adversarial camouflage.

2.1 Physical Adversarial Patch

A physical adversarial patch is a physical object or pattern that, when strategically placed or affixed to an object in the real world, can cause misclassification by computer vision systems. These patches are designed using algorithms and optimization techniques to exploit vulnerabilities in the

target system. They often incorporate features that, when perceived by the model, lead to incorrect predictions. Early adversarial patches, were employed to attack image classification [3, 13, 59] and object detection [6, 24, 32, 40, 45, 49, 54, 56] models by being strategically placed on the target objects. The Expectation Over Transformation (EOT) algorithm, as proposed by Athalye et al. [1], takes a step further in generating robust adversarial samples. This algorithm simulates real-world environmental factors, including angles, brightness, distance, and various transformation parameters, during the training process, enhancing the resilience of the adversarial patches. Lee et al. [24] successfully employed untargeted PGD [34] and the EOT [1] algorithm to generate adversarial patches that were capable of effectively attacking the YOLOv3 [38] detection algorithm in the physical world. To further enhance the robustness of adversarial patches, Xu et al. [56] introduced the Thin Plate Spline Mapping [2] technique to simulate non-rigid deformations on the surface of clothing, such as wrinkles, that occur in real-world environments. Huang et al. [21] optimized adversarial patches by introducing a set of transformations to mimic deformations and attributes. On the other hand, adversarial patches often feature strong visual appeal, which significantly impacts their concealability when applied in the physical world. Therefore, Tan et al. [43] conducted an analysis considering three aspects: color characteristics, edge features, and texture features. They utilized a projection function in conjunction to constrain the characteristics of the adversarial patch. Kung et al. [18] employed Generative Adversarial Networks (GANs) to learn image manifolds from real-world images, thereby generating physical adversarial patches for use in object detectors.

Although adversarial patches have proven effective in attacking models, it is crucial to acknowledge their limitations in terms of distance and angles. In light of these constraints, our work primarily centers on the generation of adversarial camouflage.

2.2 Physical Adversarial Camouflage

Adversarial camouflage, when applied to the surface of a target object, demonstrates sustained attack efficacy across multiple viewpoints, in contrast to adversarial patches which are effective only from specific angles and on a limited portion of the target. To optimize the camouflage on the target object’s surface, early research employed methods such as clone networks, genetic algorithms, and 3D modeling [53, 58]. For instance, Hu et al. [20] introduced the Toroidal-Cropping-based Expandable Generative Attack (TCEGA) strategy, generating adversarial textures that can be repetitively applied for attacks from various viewpoints. However, these methods did not effectively integrate non-rigid deformations of the three-dimensional object surface into the training process of textures, leading to suboptimal utilization of the target’s structural information, which is crucial for real-world

attacks. The emergence of neural rendering [23] has revolutionized adversarial camouflage by allowing mapping onto three-dimensional model surfaces, thereby recreating realistic effects in real-world scenes. Leveraging the differentiable nature of neural rendering, a considerable body of work [11, 41, 47, 48] has employed white-box methods to optimize and obtain optimal adversarial textures. However, relying on simple repetitive projection and full-coverage methods has demonstrated limited effectiveness in real-world applications. Suryanto et al. [42] enhanced the process of camouflage mapping by employing tri-planar mapping [37], thereby improving the generality and robustness of adversarial camouflage. Additionally, Hu et al. [19] utilized Voronoi diagrams and the Gumbel-softmax method to optimize camouflage textures, enhancing the texture mapping process in conjunction with 3D Thin Plate Spline transformations [2, 9, 44]. This comprehensive approach aims to address the limitations of previous methods, providing consistency and clarity in the development of effective adversarial camouflage strategies. However, in this work, a more flexible and easily implemented camouflage is proposed.

3 Flexible Physical Camouflage Generation

The difficulty of current adversarial camouflage generation is to map the 2D texture to the 3D object in a differential way. In the meantime, it is difficult to transfer the generated adversarial texture into the physical world in an alignment manner. To solve these problems, this paper proposed a new framework as previously mentioned FPA.

The structure of the work can be depicted as follows, the 3D object rendering tool we applied is a differentiable mesh renderer in which we only need to optimize the 2D texture to obtain the camouflage. Different from previous work, the structure we applied generated with the environment which can be changed dynamically with the background color style.

To achieve differential optimization of textures, we leverage the differentiable mesh renderer¹ to render the target object in a specified environment. The rendered image is then fed into object detection models such as YOLOv5 [22], YOLOv3 [38], Faster R-CNN [39], etc. In contrast to previous approaches where the texture mask is applied directly to the 3D object in a specific view, we manually define the area to be optimized using Blender. This involves selecting faces in the 3D object files that require optimization, followed by a baking procedure to map the camouflage area to a new UV map. Simultaneously, a new texture is generated post-baking, serving as the texture mask for subsequent optimization steps.

To maintain differentiability throughout the process, the differentiable mesh renderer is employed to render the texture onto the 3D object file. The renderer and associated components support batched inputs, enabling the rendering of a batch

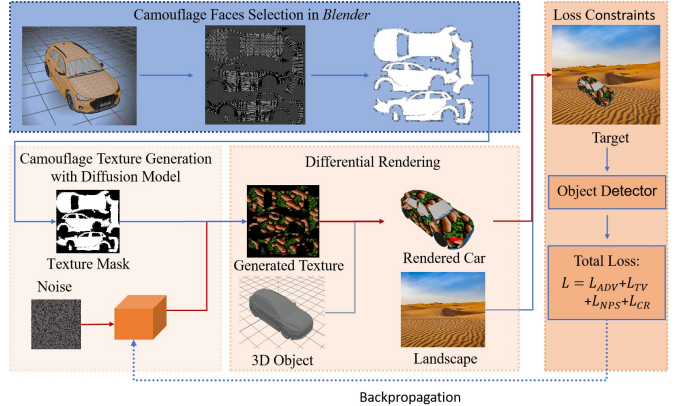


Figure 1: The workflow of the proposed framework, the red line denotes the gradient flow.

of output images in a single forward pass. The background-free nature of the rendered image from PyTorch3D poses a challenge in ensuring generalization. To address this, a fusion method is applied to seamlessly integrate the rendered object into diverse landscapes, enhancing generalization. Throughout the entire process, excluding camouflage face selection, the optimization of the adversarial texture follows an end-to-end approach, facilitated by the differentiable rendering procedure in the renderer. This framework allows for versatile texture generation methods, including gradient-based techniques (e.g., FGSM [16], PGD [34]), generative-based models (e.g., GAN [15]), and diffusion-based models, ensuring flexibility and consistency in the overall approach.

3.1 Camouflage Faces Selection

As we described before, the neural renderer usually applies the repeated manner in the camouflage pattern covering. And it is difficult to control the place or points that the camouflage attacked on. In this work, before the optimization, the Blender is applied to select the points and faces we want to cover, then the UV mapping is applied to obtain the 2D texture which is the sticker style that can stick to the target in the physical world. This procedure is achieved through texture baking which creates a new texture based on the faces selected. The texture we selected is illustrated in Figure 2.

3.2 Camouflage Texture Generation

Different from previous work, as to texture can be mapped to the target 3D object directly, therefore, in this paper, the adversarial texture of the target model can be optimized directly in the 2D space, i.e., the UV map of the texture. To ensure the texture can obtain the adversarial information and can deceive the target model, which means we can transfer the gradient among the synthetic target image, the 3D object, and the UV map, the differentiable mesh renderer is applied,

¹www.pytorch3d.org



(a) UV map of selected texture. (b) Mask image of the texture.

Figure 2: The selected camouflage area on the UV map.

and as described in section 3, the gradient information is transferring.

3.2.1 Generation with Diffusion Model

As there is a differential optimization flow for the texture generation, the diffusion-based mode can be applied to generate the adversarial texture and suppose the input is noise data ϵ which is a Gaussian distribution $N(0, I)$ generally, then the generator with U-Net as the backbone to generate the image T_k at time k , then each diffusion step can be described as follows: The generator takes the image T_k and adds Gaussian noise ϵ_k to it, where ϵ_k is a Gaussian distribution $N(0, \sigma_k^2 I)$, and σ_k is the standard deviation of the Gaussian noise at time k , which is shown as follows:

$$T_{k-1} = G_{\theta}(T_k + \epsilon_k) \quad (1)$$

where G_{θ} is the generator with U-Net as the backbone, θ represents the parameters of the generator, and k represents the time step. The generator then applies a series of convolutional operations to the noisy image to obtain a new image T_{k-1} .

3.2.2 Generation with One-Step Backward

Apart from the diffusion model to generate the adversarial texture, it can also be used one step backward to optimize the adversarial texture same as the FGSM or PGD, which injects isotropic noise into manipulated samples and using the gradients of the neural network to create adversarial examples. The optimization involves minimizing the difference between the adversarial texture and the original texture, subject to a constraint on the perturbation magnitude or perceptual sensitivity of the adversarial noise. Similarly, the texture T is the trainable parameter, then the gradient is added to T to create the perturbation. Different from the FGSM which needs to ensure the generated perturbation is small enough to be imperceptible to the human eye, the constraints of the texture include natural, similar to the background, and smooth. Therefore, the gradient is added directly in an efficient way, and this procedure can be described as follows:

$$\eta = v \nabla_T L(w, y, T_a) \quad (2)$$

Then the texture is updated with $T_a = T_a + \eta$. After the one-step updating, the new texture T_a will be differentially covered towards the target with the differentiable mesh renderer, and then the rendered image is fed into the detection model to validate whether it is adversarial or not.

3.3 Differential Rendering

The texture maps optimized through the diffusion model need to be rendered onto the corresponding regions of the 3D target for further optimization. One difficulty here is that almost all current 3D neural render methods can only process one texture, that is to say, there should only be one texture for a 3D model, otherwise, it can not be correctly rendered. To cope with this problem, the texture blending technique is applied to map different textures in a single 3D object. The texture blending technique involves blending multiple textures based on the blending factor. The blending factor is the texture index associated with each vertex. Then the linear interpolation is applied to fuse the texture, which can be expressed as $T_{blended} = \sum_i^K \lambda_i \cdot T_i$, where $T_{blended}$ is the resulting blended texture, and T_i is the original texture, and λ_i is the blending factor which is 1 in the general case.

Therefore, we utilize a texture blending approach to replace the corresponding regions in the original texture with baked textures. After the differential rendering with differentiable mesh renderer R , the fusion step is applied to join the background and the rendered object in the same picture to create the new scenario, and this procedure can be described as follows:

$$x_{adv} = R(T_{blended}, M, P, E) \cdot m_{bk} + x \cdot (1 - m_{bk}), \quad (3)$$

where M represents the model file of the target being attacked, P represents the positional information between the target and the camera, E represents environmental information (including brightness, lighting intensity, reflection parameters, etc.), and m_{bk} represents the mask image segmented out from the target (with the segmented area set to 1 and the background area set to 0). The algorithm is described in Algorithm 1. Then, the rendered batch images will be treated as training data to obtain the adversarial texture.

3.4 Loss constraints

3.4.1 Adversarial Loss

After the object detector identifies the target, it outputs predicted confidence scores and the bounding box positions. Our objective is to evade detection by the detector, thus the designed adversarial loss L_{adv} consists of two components: L_{iou} and L_{obj} . Firstly, L_{iou} is defined as the intersection over union (IOU) between the bounding boxes output by the object detector and the bounding boxes in the ground truth labels. During the non-maximum suppression process of object detection,

Algorithm 1 Differential Rendering

- 1: Set the batch size of the render images
 - 2: Load 3D object file M with “load objects as meshes”
 - 3: Load the background images x , the mask images m_{bk} ,
 - 4: Obtain the texture tensor T with “maps padded”
 - 5: Replace the stacked baked textures in T with adversarial textures T_k generated by the diffusion model.
 - 6: Create a Phong renderer by composing a rasterizer and a shader. The textured Phong shader will interpolate the texture UV coordinates for each vertex, sample from a texture image, and apply the Phong lighting model, set parameters E
 - 7: Set the range of the elevation, azimuth, and distance between the object and the camera
 - 8: **for** i in batch size **do**
 - 9: Sample the elevation, azimuth, and distance from the defined range, denoted as parameters P
 - 10: Render the image with the defined elevation, azimuth, and distance.
 - 11: Obtain the render images with Equation 3
 - 12: **end for**
-

bounding boxes with an IOU lower than a threshold are directly filtered out. Therefore, our objective is to reduce the overlap area of bounding boxes, thereby decreasing the IOU value. L_{obj} is defined as the confidence score of the bounding boxes containing the target. We identify the bounding boxes with the highest confidence score as the target and optimize towards minimizing it during the training process, thereby suppressing the recognition of the object detector. Therefore, our adversarial loss is defined as follows:

$$\begin{cases} L_{iou} = \max(\text{IOU}(y^{(x)}, b_i^{(x)})), \\ L_{obj} = \max(c^{(x)}), \\ L_{ADV} = \min(\alpha L_{iou} + \beta L_{obj}) \end{cases}, i = 1, 2, \dots, N. \quad (4)$$

In the equation, x represents the input image, y denotes the ground truth label, N is the number of output bounding boxes, c stands for the confidence score predicted by the detector, b represents the bounding boxes information predicted by the detector, and α, β are the weight coefficient.

3.4.2 Texture Smoothness

Texture smoothness is a key procedure to ensure the generated texture can be applied in the physical world with naturalness, effectiveness, and printability. As a smooth texture is more natural and realistic, making it less suspicious to human observers and more difficult to detect by deep learning systems, also improves the effectiveness of the adversarial attack by reducing the visual artifacts and noise that may interfere with the target object recognition, and is more printable and transferable to physical objects, making it easier to apply the

adversarial attack in the real world. Therefore, we propose the total variation loss in Equation 5.

$$L_{TV} = \frac{1}{N_{nz}} \sum_{i,j} (\|T_{i,j} - T_{i+1,j}\|) + (\|T_{i,j} - T_{i,j+1}\|), \quad (5)$$

where $T_{i,j}$ is the pixel value in the texture T . Different from the original TV loss, each value is decided by the mask which is whether there is a texture pattern or not, and N_{nz} is the total number of pixels in the area we selected.

3.4.3 Digital to Physical Score

It is necessary to convert the digital color to the physical world to ensure the generated texture can be applied in the physical world. The generally used method is color management to ensure the color in digital and printable spaces is the same. Let P be the set of printable colors, and let C be the set of colors in the adversarial texture. Let $d(T_i, p_j)$ be the Euclidean distance between color T_i in the texture and color p_j in the set of printable colors. Then, the non-print-ability score loss L_{NPS} is given by:

$$L_{NPS} = \sum_{i=1}^H \sum_{j=1}^W \min_{p_j \in P} d(T_{i,j}, p_j), \quad (6)$$

where H and W are the height and width of the adversarial texture, respectively. The goal of the optimizer is to minimize the non-printability score loss, along with other loss functions such as the total variation loss and objectness score loss, to generate an adversarial texture that can be physically printed and placed on an object to fool an object detection system.

3.4.4 Concealment Constraint

We propose a concealment constraint loss to ensure the similarity between the generated texture and the background, enhancing the dual concealment of texture in both machine vision and human visual observation. First, we compute the average RGB value c_r within the background region based on the target. Based on the set color fluctuation threshold c_{ru} , the range of background color variation can be obtained as $[u_l, u_h]$, where $u_l = c_r - c_{ru}$ and $u_h = c_r + c_{ru}$. Then, we compute the difference between the generated texture and the background color variation to construct the concealment constraint loss, which can be represented as Equation 7.

$$L_{CR} = \frac{1}{M} \sum_{i,j} \|T_{i,j} - u_l\| + \|T_{i,j} - u_h\|, \quad (7)$$

where M denotes the total number of the nonzero pixels, $T_{i,j}$ represents the pixel value of adversarial texture at coordinate (i, j) , lower L_{CR} indicates closer resemblance between the texture color and the background. Thus, minimizing L_{CR} enhances the similarity between texture color and background, thereby improving concealment in the environment.

The total loss of adversarial training is described by Equation 8, γ, μ, τ are the weights to balance loss.

$$L = L_{ADV} + \gamma L_{TV} + \mu L_{NPS} + \tau L_{CR} \quad (8)$$

The training procedure is described in Algorithm 2.

Algorithm 2 Image optimization with diffusion model

- 1: Load object detection model as the target model \mathbf{O}
 - 2: Obtain the input image x , the ground truth y
 - 3: **for** step in STEPS **do**
 - 4: **for** k in Diffusion STEPS **do**
 - 5: Obtain the adversarial texture T_k with Equation 1
 - 6: Obtain the rendered image x_k with Algorithm 1
 - 7: **end for**
 - 8: $b^{(x)}, c^{(x)} = \mathbf{O}(x_k, y^{(x)})$
 - 9: Obtain the adversarial loss with Equation 4
 - 10: Obtain the smooth variants with Equation 5
 - 11: Obtain the color constraints with Equation 6
 - 12: Obtain the concealment constraints with Equation 7
 - 13: Set L by Equation 8
 - 14: Update diffusion model parameters θ for minimizing L by via backpropagation
 - 15: **end for**
-

4 Experiments

In this section, we first introduce the foundational configuration of the experiments, including experimental parameters, datasets, object detection algorithms, evaluation metrics, and more. Then, combining simulations and real-world environments, we conduct a thorough and adequate assessment of camouflage.

4.1 Experimental Settings

Datasets To ensure the effectiveness of physical world attacks, we conducted experiments using a dataset collected based on the CARLA simulator [10]. To facilitate fair comparisons with prior adversarial camouflage works, we directly employed the same dataset as (FCA [47]). The dataset was gathered in modern urban environments provided by CARLA, encompassing various distances, pitch angles, and yaw angles. The training set comprises 12,500 images, while the validation set consists of 3,000 images. Furthermore, to validate the superiority of our framework and loss function in camouflage concealment, we conducted experiments based on the Place365 dataset, selecting three common scenarios (grassland, desert, and highway). Each scene’s training set comprises 50 background images, and the validation set comprises 10 images.

Target Models To evaluate the adversarial camouflage’s attack performance, we selected commonly used detection

models of different architectures for experimentation. Specifically, these include single-stage detection algorithms such as SSD [31], YOLOv3 [38], YOLOv5 [22], and YOLOv7 [46], as well as two-stage detection algorithms like Faster R-CNN(FRCNN) [39], Mask R-CNN(MkRCNN) [17], and Cascade R-CNN(CaRCNN) [4]. Additionally, we included detection algorithms based on Transformer architecture, namely DETR [5] and RT-DETR [33]. Among these, SSD and Faster R-CNN were pretrained on the VOC2007 dataset [12], while the remaining detection models were pretrained on the COCO dataset [30].

Evaluation Metrics For object detection models, AP@0.5 is commonly used to evaluate the recognition capability of the models. We set the value of AP@0.5 at an IoU threshold of 0.5 as the first evaluation metric for assessing attack performance. The purpose of adversarial camouflage is to conceal the target vehicle and evade detection by the object detector. Therefore, we collect all candidate boxes detected by the detector for each image, and if the confidence scores of all candidate boxes are below the threshold $\text{conf}=0.5$, the image is considered successfully attacked. The second evaluation metric is the Attack Success Rate (ASR), defined as the proportion of successfully attacked images among all test images.

Implementation Details In the actual deployment of adversarial camouflage, there is a process of magnification and printing. To minimize the loss of details in adversarial camouflage, considering the existing hardware conditions, we set a higher resolution for the adversarial camouflage, with an initial size of 480*480. The adversarial camouflage uses the same random seed for each training iteration, initialized with random noise. We employ Adam as the optimizer with default parameters, a learning rate of 0.001, and a maximum of 10 epochs. The parameters of the loss function are configured based on extensive experimental experience, with the following settings: $\alpha = 0.05$, $\beta = 1.0$, $\gamma = 1.0$, $\mu = 2.5$, $\tau = 2.0$. All our code is implemented in PyTorch and training/validation are conducted on an NVIDIA GeForce RTX 3090 GPU.

4.2 Universality Evaluations

Transferability Evaluation Across Different Victim Models We trained adversarial camouflages against different victim models: FPA(v3) against YOLOv3, FPA(v5) against YOLOv5, and FPA(FR) against FRCNN. To ensure a fair comparison with prior adversarial camouflage works, we validated our approach using the same dataset as FCA. We added 5 groups of adversarial camouflages as comparative experiments: Noise, CAMOU [57], ER [53], DAS [48], FCA [47]. Among these, CAMOU and ER adversarial camouflage cover the entire vehicle by repeated pasting. For DAS and FCA adversarial camouflage, we employed the same neural rendering technique as the original paper, overlaying textures onto the vehicle surface through neural rendering. As shown in Fig-

ure.3, vehicles covered by our trained adversarial camouflage interfere with detector recognition and demonstrate the most effective attack. Table.1 presents the comparison results of adversarial camouflage on AP@0.5. Our method achieves the best results across multiple detection models. Specifically, on YOLOv3, FPA(v5) exhibits the maximum drop of 73.9% in AP@0.5, surpassing FCA by 10%. On the widely used YOLOv5, it achieves an 89.1% reduction, indicating the concealment capability of our camouflage at any angle. Due to the architectural differences of FRCNN and the diversity of training datasets for detection models, the effectiveness of FPA (v5) in attacks slightly decreased, yet it still achieved a 52% reduction, surpassing other real-world attack methods. When employing FRCNN as the victim model, our adversarial camouflage, FPA(FR), achieved a reduction of 74.9%. The last column in the table indicates the average decrease in AP@0.5 across the three detectors, with our method achieving the best results. Particularly, FPA(v5) achieved a reduction of 71.6%, demonstrating the ability of our framework to generate highly aggressive camouflage when facing different victim detection models.

Table 1: The comparison results of AP@0.5 for adversarial camouflage generated based on different victim models. The "Drop↓" column indicates the average decrease in AP@0.5 of the adversarial camouflage across the three detectors.

Method	YOLOv3	YOLOv5	FRCNN	Drop↓
RAW	0.898	0.979	0.839	0.000
Noise	0.672	0.781	0.622	0.214
CAMOU	0.660	0.654	0.581	0.274
ER	0.743	0.804	0.734	0.145
DAS	0.803	0.916	0.833	0.054
FCA	0.265	0.563	0.545	0.448
FPA(v3)	0.212	0.343	0.487	0.558
FPA(v5)	0.159	0.088	0.319	0.716
FPA(FR)	0.543	0.513	0.090	0.523

Transferability Evaluation Across Different Architecture Detectors To assess the effectiveness of adversarial camouflage on unknown models, we introduced several different architectures of detection models, including SSD, YOLOv7, Mask R-CNN(MkRCNN), Cascade R-CNN(CaRCNN), DETR, and RT-DETR. The test results for AP@0.5 are shown in Table.2, where our adversarial camouflage, FPA(v5), outperforms others on every detection model. In the latest detection model YOLOv7, it achieves a significant reduction from the original 97.9% to 11.2%, demonstrating robust attack effectiveness. When confronted with CaRCNN, while other camouflage methods only slightly decrease AP@0.5, our adversarial camouflage, FPA(v5), achieves a reduction of 48.2%. Interestingly, when facing detection models based on Transformer architecture, our attack method also demonstrates strong attack capability, achieving a reduction of

68.3% in DETR. This indicates the robustness of our method against unknown architectures of black-box models. Figure.4 illustrates the prediction results of our adversarial camouflage, FPA(v5), across different detection models. Our method enables vehicles to evade detection model recognition, further validating the robust transferability of our approach.

Transferability Evaluation Across Different Tasks We aim for the adversarial camouflage, once covering the vehicle, to not only impact target detection recognition but also disrupt other tasks, such as depth estimation commonly used in the field of autonomous driving. We validate the attack performance of the adversarial camouflage on publicly trained depth estimation models, including Monodepth2 (MoD for short) [14], Depth Hints (DH for short) [51], and ManyDepth (MaD for short) [52]. For a more comprehensive evaluation, we generated 24 test images based on different environments at distances of 5 meters and 10 meters. Additionally, we selected two common metrics on depth estimation, depth error(\mathcal{E}_d), and the proportion of affected regions(\mathcal{R}_a) [7]. The experimental results, as presented in Table.3, indicate that our attack achieves the best performance on MoD, with a depth influence of 12.36 and a proportion of affected regions reaching 85.4%. Figure.5 illustrates the prediction results on MoD. After applying the adversarial camouflage, the display of the original vehicle depth almost completely disappears, further confirming the strong transferability of our method across different tasks.

4.3 Simulation Evaluation of Physical World Factors

Robustness Evaluation at Different Locations In the physical world, different distances and angles can significantly affect the effectiveness of adversarial camouflage. To validate the robustness of our adversarial camouflage to positional changes, we utilized images generated using PyTorch3D rendering (pure background) for evaluation. Specifically, most previous studies did not conduct validation at longer distances. To comprehensively evaluate the adversarial camouflage, the distances of the images we collected include [5, 10, 20, 30, 40, 50]. We captured images every 3 degrees within a 360° range, with a fixed range of pitch angles [0, 10, 20, 30, 40, 50], resulting in a total of 4320 images. Validation results are shown in Figure.6, evaluated based on distance, pitch angle, and azimuth angle. To better represent the validation results, azimuth angles are evaluated within a range of 45° increments. Note that as the distance increases, the recognition capability of the target detection model is affected beyond 40 meters. We found that at 40 meters, the ASR of the detection model on the original vehicle is 2.92%, while at 50 meters, it is 15.14%. Meanwhile, we noticed a slight decrease in ASR after 10 meters, followed by an increase after 40 meters, with overall fluctuations within a small range as the distance increases. Due to the partial coverage of our camouflage, which

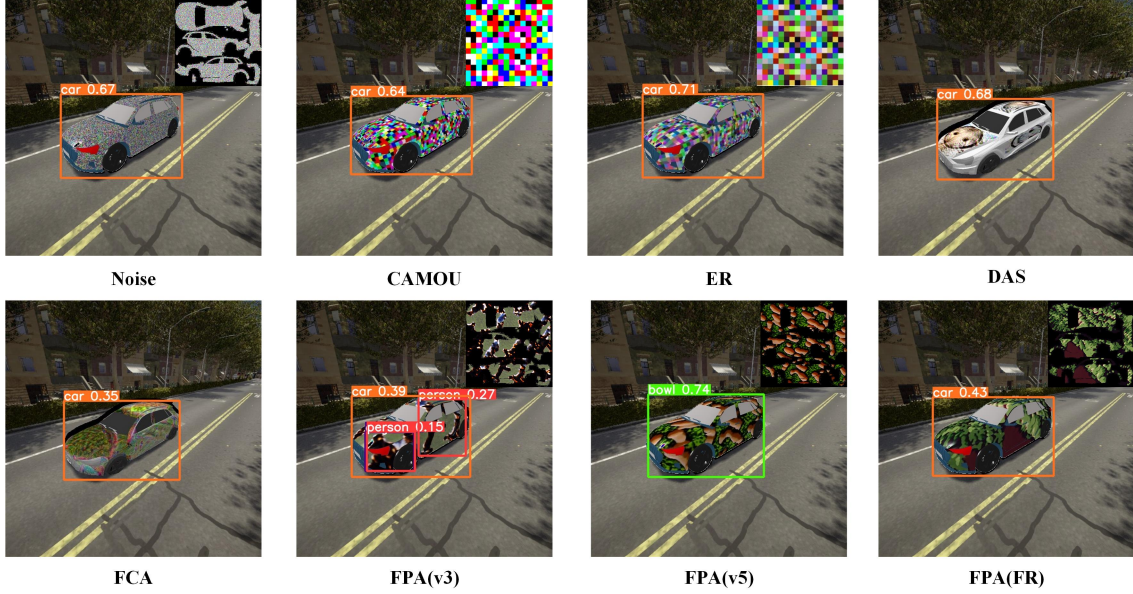


Figure 3: The presentation of adversarial camouflage and the prediction results under the YOLOv5 detection model.

Table 2: The AP@0.5 test results of adversarial camouflage under different detection models.

Methods	Single-Stage		Two-Stage		Transformer	
	SSD	YOLOv7	MkRCNN	CaRCNN	DETR	RT-DETR
RAW	0.846	0.979	0.961	0.988	0.969	0.798
Noise	0.716	0.874	0.917	0.968	0.719	0.426
CAMOU	0.447	0.831	0.849	0.967	0.854	0.251
ER	0.503	0.896	0.899	0.978	0.866	0.309
DAS	0.618	0.763	0.633	0.885	0.745	0.672
FCA	0.205	0.259	0.597	0.872	0.389	0.257
FPA(v3)	0.197	0.358	0.476	0.756	0.138	0.081
FPA(v5)	0.179	0.112	0.406	0.506	0.286	0.053
FPA(FR)	0.117	0.481	0.616	0.847	0.400	0.200

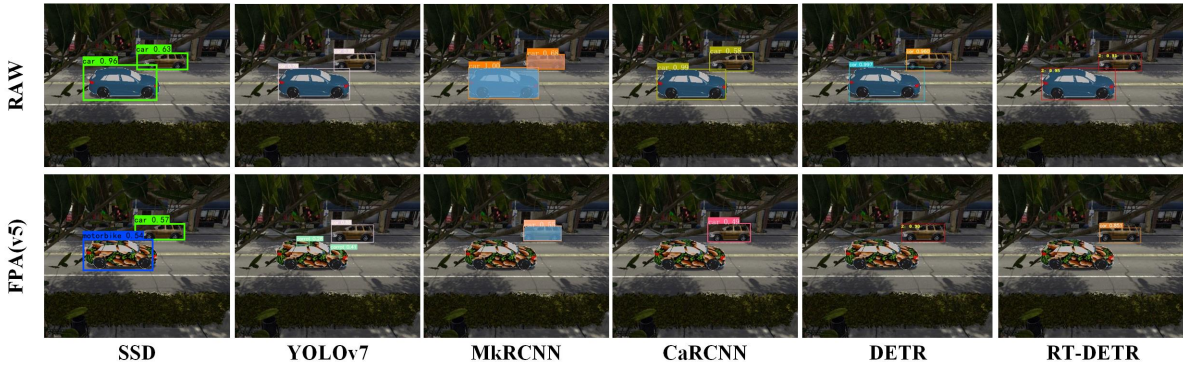


Figure 4: The first row shows the prediction results of original samples under various detectors, and the second row shows the prediction results of our adversarial camouflage, FPA(v5).

does not completely conceal parts of the vehicle such as tires, windows, and grilles, images captured from certain angles with more of these features may result in a slight decrease in

ASR. Nonetheless, under angle variations, the lowest ASR can reach up to 70.83%, indicating that our method exhibits good robustness across different positions.

Table 3: Results of depth error and the proportion of affected regions testing on trained depth estimation models after applying camouflage coverage.

Evaluation Metrics	MoD	DH	MaD
\mathcal{E}_d	12.36	7.07	7.88
\mathcal{R}_a	85.40	73.93	91.76

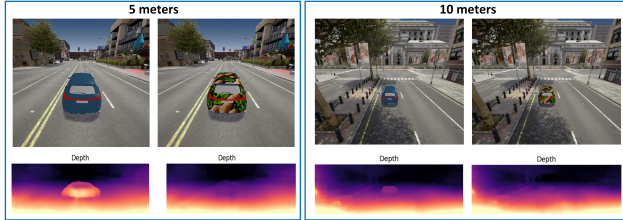


Figure 5: The prediction results of the original vehicle and the vehicle covered with our adversarial camouflage under the depth estimation model.

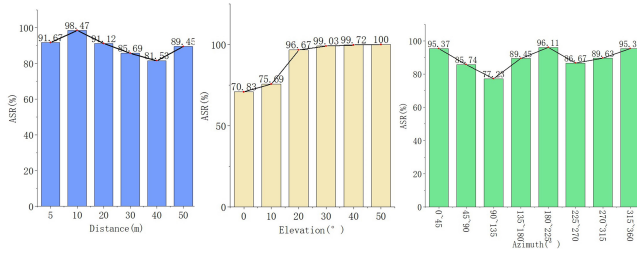


Figure 6: The ASR test results under different distances, pitch angles, and azimuth angles.

Robustness Evaluation under Different Occlusions In the physical world, targets often appear partially visible in images, leading to partial camouflage coverage. Therefore, we conducted experiments to evaluate the robustness of our method under different degrees of occlusion. To prevent images from becoming too small after occlusion, we set the distance range to [5, 10, 15, 20], pitch angles to [15, 30, 45, 60], and collected images at intervals of 12° within a 360° angle range. To generate rendered images with different occlusion levels, we start with the width of the target as the initial length and occlude it from left to right in 10 equal proportions from 0 to 1. Meanwhile, we designate proportions from 0.1 to 0.3 as small occlusion, proportions from 0.4 to 0.6 as middle occlusion, and proportions from 0.7 to 0.9 as large occlusion. Hence, each data point in Table.4 represents the ASR calculated across 360 test images. In Figure.7, we present the prediction results under occlusion ratios of [0.1, 0.4, 0.7]. From the data in the table, it is evident that our camouflage achieves an ASR close to 100% under different occlusion areas, indicating the strong robustness of our method against occlusion.

Robustness Evaluation under Different Reflection Coef-

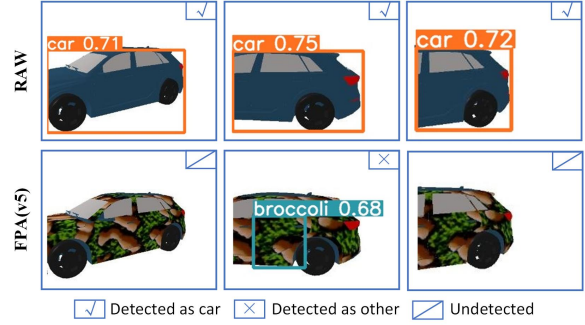


Figure 7: The prediction results of the original car and the camouflaged car under YOLOv5. The ticked box indicates a correct recognition result, the crossed box indicates a recognition error, and the slashed box indicates no recognition result.

icients The intensity of lighting in the physical world can significantly affect adversarial camouflage. This is primarily because varying light intensities can result in different degrees of reflection on the surface of the vehicle, consequently altering the camouflage. Our method simulates physical parameters during the training process of adversarial camouflage using PyTorch3D, ensuring robustness in real-world environments. Therefore, in this section of the experiment, we used PyTorch3D to set the reflectivity coefficient(diffuse_color) of the target surface, simulating the reflection of the target under different conditions. Specifically, we defined a set of reflectivity coefficients [1.0, 3.0, 5.0, 10.0, 15.0] for experimentation. The data collection method was the same as the occlusion experiment. Each value in Table.5 is calculated based on ASR from 480 test images. From the data in the table, we can find that the ASR of adversarial camouflage fluctuates around 97% and is very little affected by reflection. The graph depicted in Figure.8 illustrates that the camouflaged vehicle successfully evades detection by the target detection system, indicating that our method exhibits good robustness across different reflectivity coefficients.

4.4 Concealment Evaluation

The purpose of camouflage is to reduce the optical contrast between the target and the background, thereby increasing the similarity between the target and the background, and thus achieving the concealment of the target. Therefore, in adversarial camouflage, we not only need to effectively attack the target detection model but also ensure that the camouflage maintains a level of similarity with the background, enhancing visual concealment. Most previous work on the concealment of adversarial camouflage [18, 29] relied on subjective observational experiments to measure the effectiveness of target camouflage, lacking scientific and accurate assessment. We conducted experiments based on digital image analysis

Table 4: The ASR test results of the adversarial camouflage under different occlusion ranges.

Occlusion range	Distance							
	5		10		15		20	
	RAW	FPA(v5)	RAW	FPA(v5)	RAW	FPA(v5)	RAW	FPA(v5)
None	1.67	100	0.00	100	0.00	100	0.00	98.33
Small	18.06	100	3.05	100	4.17	100	7.23	99.45
Middle	44.45	100	30.39	100	39.67	100	56.67	100
Large	86.12	100	82.23	100	84.34	100	89.37	100

Table 5: The ASR test results of the adversarial camouflage under different reflective coefficient settings.

diffuse_color	1	3	5	10	15
RAW	1.67	1.67	1.25	0.00	0.83
FPA(v5)	97.91	97.71	97.08	96.25	96.87

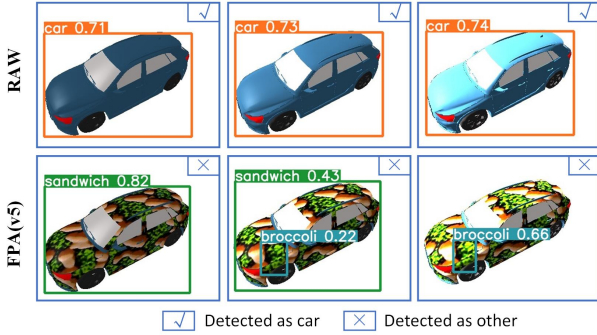


Figure 8: Rendered images (from left to right) at reflectance factors of 1.0, 5.0, and 15.0, and predicted results under YOLOv5.

techniques to comprehensively and accurately analyze the effectiveness of camouflage, focusing on model attention and image similarity.

Evaluation of Model Attention We analyze the interference of adversarial camouflage on model attention using the Grad-CAM visualization tool. Grad-CAM utilizes a pre-trained ResNet50 as the base model for recognizing images. The findings depicted in Figure.9 reveal a noteworthy pattern: the model’s attention predominantly centers around the original vehicle, with minimal focus directed towards the camouflaged vehicle. This observation underscores the disruptive effect of adversarial camouflage, effectively diffusing the model’s attention away from the intended target.

Evaluation of Image Similarity In the constructed scene dataset, we adopt two training modes: Camou-raw, which does not include the L_{CR} , and Camou-color, which includes the L_{CR} . We generated adversarial camouflage for three different scenarios. To analyze the camouflage effectiveness more

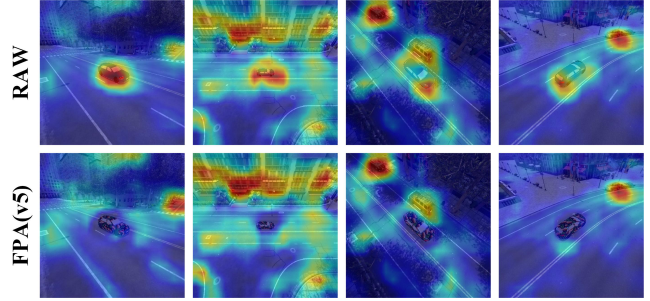


Figure 9: The attention distribution results generated by Grad-CAM for the original and camouflaged vehicles.

scientifically and accurately, we propose two metrics based on image similarity: Color Similarity (CSIM) and Structural Similarity (SSIM) [50]. Specifically, we first compute the color histograms of the two images. Then, we calculate the histogram difference using the Bhattacharyya distance [8] to obtain the color similarity. A smaller value indicates that the colors of the two images are more similar. We compute the similarity between the target and the background within ranges of 5m, 10m, and 20m, and validate it in the constructed dataset. The results are shown in Figure.10. In

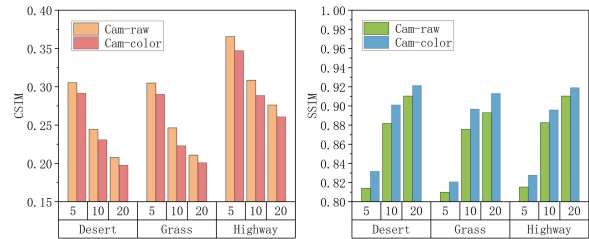


Figure 10: The comparison of similarity between adversarial camouflages generated under two training modes in desert, grassland, and highway scenarios.

all three scenarios, the adversarial camouflage generated by Camou-color achieved better results in both SSIM and CSIM. Table.6 presents the ASR results of adversarial camouflage under different training modes in YOLOv5, where “None” indicates the detection results of the vehicle without camouflage. The attack effectiveness of adversarial camouflage

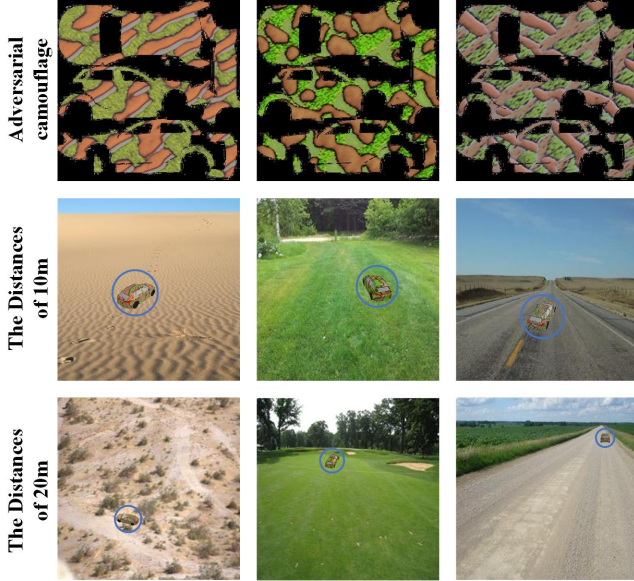


Figure 11: The first row illustrates the adversarial camouflage across various scenarios obtained through Camou_color training. The second and third rows display the rendered results of the camouflaged car at distances of 10m and 20m, respectively.

under the Camou-color training mode is slightly lower compared to Camou-raw, but both can significantly impact the target detection model. Figure.11 illustrates rendered images of vehicles concealed with camouflage across different scenarios. Visually, these images create confusion, indicating that our method significantly enhances camouflage concealment while maintaining attack effectiveness.

Table 6: The original vehicle, along with the ASR test outcomes of the adversarial camouflage in various scenarios obtained through the two training methodologies.

Method	Desert	Grass	Highway
None	0.50	0.35	0.77
Camou-raw	91.08	92.59	87.86
Camou-color	83.56	87.27	84.89

4.5 Physical World Evaluation

In this section, we evaluated the adversarial camouflage’s performance in the physical world. Specifically, we conducted experiments in the physical world using a 1:24 scale Audi Q5 car model. Due to budget and time constraints, we utilized an HP color printer to print our adversarial camouflage FPA(v5), and then cut and pasted the camouflage parts onto the corresponding areas of the car model. We captured surround shots of the target at three different distances within three distinct

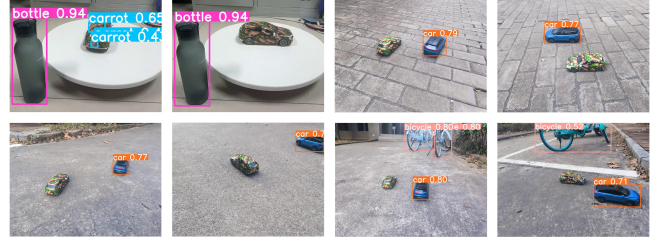


Figure 12: The prediction results of the original model car and the camouflaged car in the physical world.

environments to assess the efficacy of camouflage, utilizing the Redmi K50 Pro as the imaging device. The original and camouflaged cars were captured using the same model for data collection. From the collected data, we extracted 200 images for validation purposes, with the AP@0.5 results presented in Table.7, and a selection of prediction outcomes illustrated in Figure.12. Our adversarial camouflage significantly reduces AP@0.5 across various detection models, particularly in SSD, showing a reduction of up to 82.5%. This indicates that our method can effectively overcome physical world interference and efficiently attack object detection models.

4.6 Ablation Studies

In this section of the experiment, we investigated the effects of different training methods (including diffusion model modules, and initialization areas) and loss function terms on adversarial camouflage.

Different Combinations of Loss Functions. We investigated the impact of different combinations of loss functions on adversarial camouflage, including L_{attack} , $L_{attack} + L_{vt}$, and $L_{attack} + L_{nps}$ for validation. Meanwhile, we compared the AP@0.5 computed on the test set collected based on Carla. The experimental results are presented in Table.8, indicating a decrease in the performance of adversarial camouflage in the absence of certain loss function terms. When considering only the L_{attack} term, the attack effectiveness surpasses the other two experimental groups. However, as depicted in Figure.13, the absence of the L_{vt} term leads to numerous black spots in the camouflage, resulting in reduced concealment. Conversely, the lack of the L_{nps} constraint results in brighter camouflage colors, leading to significant pixel information loss during printing. Therefore, by combining L_{attack} , L_{nps} , and L_{vt} , we achieve stronger attack performance and better concealment for the adversarial camouflage.

Different Training Methods In this section, we investigate the impact of the diffusion model on optimizing against camouflage and the effect of the initialization area on the attack’s effectiveness. We establish two optimization methods: traditional gradient-based optimization and diffusion model-based optimization as described in Section 3.2. Meanwhile, two methods of initial area change are set, local coverage and

Table 7: The AP@0.5 test results of the original car and the camouflaged car in the physical world.

Method	SSD	Yolov5	FRCNN	MkRCNN	DETR	RT-DETR
RAW	0.930	0.995	0.995	0.989	0.985	0.977
FPA(v5)	0.105	0.451	0.529	0.475	0.251	0.488

Table 8: The comparison results of AP@0.5 under different loss function combination schemes.

Method	YOLOv3	YOLOv5	FRCNN	DETR
L_{attack}	0.286	0.226	0.442	0.284
$L_{attack} + L_{vt}$	0.626	0.534	0.612	0.780
$L_{attack} + L_{nps}$	0.506	0.281	0.468	0.416
$L_{attack} + L_{vt} + L_{nps}$	0.159	0.088	0.319	0.286

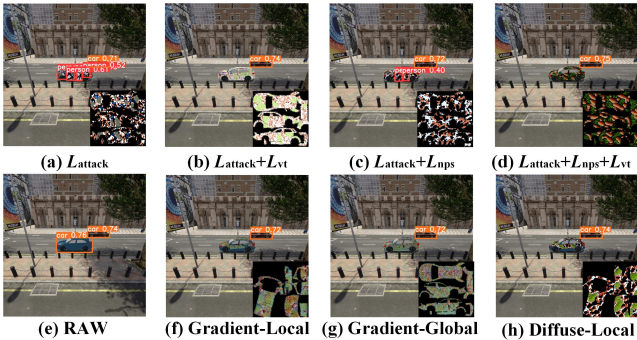


Figure 13: Confrontation camouflage display and prediction results in different settings.

global coverage. Local coverage refers to partial regions on structures such as car doors and roofs, while global coverage refers to the camouflage covering the entire vehicle (excluding structures such as windows and tires). Specifically, based on the training data collected from Carla and using YOLOv5 as the victim detection model, we generated four sets of adversarial camouflages:

- Gradient-Local: Adversarial camouflage generated based on gradient optimization and local coverage.
- Gradient-Global: Adversarial camouflage generated based on gradient optimization and global coverage.
- Diffuse-Local: Adversarial camouflage generated based on diffusion model optimization and local coverage.
- Diffuse-Global: Adversarial camouflage generated based on diffusion model optimization and global coverage.

Where Diffuse-Global represents the FPA(v5) adversarial camouflage used in the previous comparison. The AP@0.5 results of the adversarial camouflage under different detection models are presented in Table.9. It is observed that the diffusion model optimization approach significantly outperforms

the gradient approach. Meanwhile, enlarging the coverage area significantly enhances the effectiveness of camouflage. As observed in Figure.13, both gradient and diffusion model optimization-based camouflages effectively conceal the car, underscoring the robustness of our training methodology and the design of loss functions.

Table 9: Comparison of the AP@0.5 results of adversarial camouflages generated by different optimization methods and initial areas under different detection models.

Method	YOLOv3	YOLOv5	FRCNN	DETR
Gradient-Local	0.676	0.565	0.681	0.785
Gradient-Global	0.527	0.493	0.605	0.664
Diffuse-Local	0.481	0.415	0.536	0.436
Diffuse-Global	0.159	0.088	0.319	0.286

5 Conclusion

In conclusion, our work presents a novel approach to adversarial camouflage through the integration of a comprehensive 3D rendering framework, departing from conventional neural rendering methods. Leveraging the inherent capabilities of the framework, we achieved a nuanced representation of 3D targets by simulating authentic lighting conditions and material variations, thereby contributing to a more realistic rendering outcome. The combination of a generatively learned adversarial pattern from diffusion models, along with a designed adversarial loss and covert constraint loss, ensures the adversarial and covert nature of the camouflage in the physical world. The contribution of our work lies in the establishment of a rendering system rooted in a robust 3D framework, which enhances rendering efficiency and enables the generation of adversarial camouflage in sticker mode for practical deployment. The incorporation of confrontation loss and concealment constraint loss further strengthens the aggressiveness and concealment of the camouflage, demonstrating adaptability across diverse environments. In future works, we aim to explore additional deployment scenarios, and evaluate the generalization of our approach to different objects and environments, thereby advancing the field of adversarial camouflage in both theoretical and practical dimensions.

Acknowledgments

This research is supported by the xxx.

References

- [1] Anish Athalye, Logan Engstrom, Andrew Ilyas, and Kevin Kwok. Synthesizing robust adversarial examples. In *International Conference on Machine Learning*, pages 284–293. Proceedings of Machine Learning Research, 2018.
- [2] Fred L. Bookstein. Principal warps: Thin-plate splines and the decomposition of deformations. *IEEE Transactions on Pattern Analysis and Machine Intelligence*, 11(6):567–585, 1989.
- [3] Tom B Brown, Dandelion Mané, Aurko Roy, Martín Abadi, and Justin Gilmer. Adversarial patch. *arXiv preprint arXiv:1712.09665*, 2017.
- [4] Zhaowei Cai and Nuno Vasconcelos. Cascade r-cnn: Delving into high quality object detection. In *Proceedings of the IEEE conference on Computer Vision and Pattern Recognition*, pages 6154–6162, 2018.
- [5] Nicolas Carion, Francisco Massa, Gabriel Synnaeve, Nicolas Usunier, Alexander Kirillov, and Sergey Zagoruyko. End-to-end object detection with transformers. In *European Conference on Computer Vision*, pages 213–229. Springer, 2020.
- [6] Shang-Tse Chen, Cory Cornelius, Jason Martin, and Duen Horng Chau. Shapeshifter: Robust physical adversarial attack on faster r-cnn object detector. In *Machine Learning and Knowledge Discovery in Databases: European Conference, ECML PKDD 2018, Dublin, Ireland, September 10–14, 2018, Proceedings, Part I 18*, pages 52–68. Springer, 2019.
- [7] Zhiyuan Cheng, James Liang, Hongjun Choi, Guan hong Tao, Zhiwen Cao, Dongfang Liu, and Xiangyu Zhang. Physical attack on monocular depth estimation with optimal adversarial patches. In *European Conference on Computer Vision*, pages 514–532. Springer, 2022.
- [8] Euisun Choi and Chulhee Lee. Feature extraction based on the bhattacharyya distance. *Pattern Recognition*, 36(8):1703–1709, 2003.
- [9] Gianluca Donato and Serge Belongie. Approximate thin plate spline mappings. In *Computer Vision—ECCV 2002: 7th European Conference on Computer Vision Copenhagen, Denmark, May 28–31, 2002 Proceedings, Part III 7*, pages 21–31. Springer, 2002.
- [10] Alexey Dosovitskiy, German Ros, Felipe Codevilla, Antonio Lopez, and Vladlen Koltun. Carla: An open urban driving simulator. In *Conference on Robot Learning*, pages 1–16. Proceedings of Machine Learning Research, 2017.
- [11] Yexin Duan, Jialin Chen, Xingyu Zhou, Junhua Zou, Zhengyun He, Wu Zhang, and Zhisong Pan. Dpa: Learning robust physical adversarial camouflages for object detectors. *arXiv preprint arXiv:2109.00124*, 2, 2021.
- [12] Mark Everingham and John Winn. The pascal visual object classes challenge 2007 (voc2007) development kit. *Int. J. Comput. Vis.*, 88(2):303–338, 2010.
- [13] Kevin Eykholt, Ivan Evtimov, Earlene Fernandes, Bo Li, Amir Rahmati, Chaowei Xiao, Atul Prakash, Tadayoshi Kohno, and Dawn Song. Robust physical-world attacks on deep learning visual classification. In *Proceedings of the IEEE Conference on Computer Vision and Pattern Recognition*, pages 1625–1634, 2018.
- [14] Clément Godard, Oisín Mac Aodha, Michael Firman, and Gabriel J Brostow. Digging into self-supervised monocular depth estimation. In *Proceedings of the IEEE/CVF International Conference on Computer Vision*, pages 3828–3838, 2019.
- [15] Ian Goodfellow, Jean Pouget-Abadie, Mehdi Mirza, Bing Xu, David Warde-Farley, Sherjil Ozair, Aaron Courville, and Yoshua Bengio. Generative adversarial networks. *Communications of the ACM*, 63(11):139–144, 2020.
- [16] Ian J Goodfellow, Jonathon Shlens, and Christian Szegedy. Explaining and harnessing adversarial examples. *arXiv preprint arXiv:1412.6572*, 2014.
- [17] Kaiming He, Georgia Gkioxari, Piotr Dollár, and Ross Girshick. Mask r-cnn. In *Proceedings of the IEEE International Conference on Computer Vision*, pages 2961–2969, 2017.
- [18] Yu-Chih-Tuan Hu, Bo-Han Kung, Daniel Stanley Tan, Jun-Cheng Chen, Kai-Lung Hua, and Wen-Huang Cheng. Naturalistic physical adversarial patch for object detectors. In *Proceedings of the IEEE/CVF International Conference on Computer Vision*, pages 7848–7857, 2021.
- [19] Zhanhao Hu, Wenda Chu, Xiaopei Zhu, Hui Zhang, Bo Zhang, and Xiaolin Hu. Physically realizable natural-looking clothing textures evade person detectors via 3d modeling. In *Proceedings of the IEEE/CVF Conference on Computer Vision and Pattern Recognition*, pages 16975–16984, 2023.

- [20] Zhanhao Hu, Siyuan Huang, Xiaopei Zhu, Fuchun Sun, Bo Zhang, and Xiaolin Hu. Adversarial texture for fooling person detectors in the physical world. In *Proceedings of the IEEE/CVF Conference on Computer Vision and Pattern Recognition*, pages 13307–13316, 2022.
- [21] Lifeng Huang, Chengying Gao, Yuyin Zhou, Cihang Xie, Alan L Yuille, Changqing Zou, and Ning Liu. Universal physical camouflage attacks on object detectors. In *Proceedings of the IEEE/CVF Conference on Computer Vision and Pattern Recognition*, pages 720–729, 2020.
- [22] Glenn Jocher, Ayush Chaurasia, Alex Stoken, Jirka Borovec, Yonghye Kwon, Kalen Michael, Jiacong Fang, Zeng Yifu, Colin Wong, Diego Montes, et al. ultralytics/yolov5: v7. 0-yolov5 sota realtime instance segmentation. *Zenodo*, 2022.
- [23] Hiroharu Kato, Yoshitaka Ushiku, and Tatsuya Harada. Neural 3d mesh renderer. In *Proceedings of the IEEE Conference on Computer Vision and Pattern Recognition*, pages 3907–3916, 2018.
- [24] Mark Lee and Zico Kolter. On physical adversarial patches for object detection. arxiv. *arXiv preprint arXiv:1906.11897*, 2019.
- [25] Xiangjuan Li, Yang Li, Zhaowen Feng, Zhaoxuan Wang, and Quan Pan. Ats-o2a: A state-based adversarial attack strategy on deep reinforcement learning. *Computers & Security*, 129:103259, 2023.
- [26] Yang Li, Quan Pan, and Erik Cambria. Deep-attack over the deep reinforcement learning. *Knowledge-Based Systems*, 250:108965, 2022.
- [27] Yang Li, Quan Pan, Zhaowen Feng, and Erik Cambria. Few pixels attacks with generative model. *Pattern Recognition*, 144:109849, 2023.
- [28] Yang Li, Wei Zhao, Erik Cambria, Suhang Wang, and Steffen Eger. Graph routing between capsules. *Neural Networks*, 143:345–354, 2021.
- [29] Shuo-Yen Lin, Ernie Chu, Che-Hsien Lin, Jun-Cheng Chen, and Jia-Ching Wang. Diffusion to confusion: Naturalistic adversarial patch generation based on diffusion model for object detector. *arXiv preprint arXiv:2307.08076*, 2023.
- [30] Tsung-Yi Lin, Michael Maire, Serge Belongie, James Hays, Pietro Perona, Deva Ramanan, Piotr Dollár, and C Lawrence Zitnick. Microsoft coco: Common objects in context. In *Computer Vision–ECCV 2014: 13th European Conference, Zurich, Switzerland, September 6–12, 2014, Proceedings, Part V 13*, pages 740–755. Springer, 2014.
- [31] Wei Liu, Dragomir Anguelov, Dumitru Erhan, Christian Szegedy, Scott Reed, Cheng-Yang Fu, and Alexander C Berg. Ssd: Single shot multibox detector. In *Computer Vision–ECCV 2016: 14th European Conference, Amsterdam, The Netherlands, October 11–14, 2016, Proceedings, Part I 14*, pages 21–37. Springer, 2016.
- [32] Xin Liu, Huanrui Yang, Ziwei Liu, Linghao Song, Hai Li, and Yiran Chen. Dpatch: An adversarial patch attack on object detectors. *arXiv preprint arXiv:1806.02299*, 2018.
- [33] Wenyu Lv, Shangliang Xu, Yian Zhao, Guanzhong Wang, Jinman Wei, Cheng Cui, Yuning Du, Qingqing Dang, and Yi Liu. Detsr beat yolos on real-time object detection. *arXiv preprint arXiv:2304.08069*, 2023.
- [34] Aleksander Madry, Aleksandar Makelov, Ludwig Schmidt, Dimitris Tsipras, and Adrian Vladu. Towards deep learning models resistant to adversarial attacks. *arXiv preprint arXiv:1706.06083*, 2017.
- [35] Kaleel Mahmood, Rigel Mahmood, and Marten Van Dijk. On the robustness of vision transformers to adversarial examples. In *Proceedings of the IEEE/CVF International Conference on Computer Vision*, pages 7838–7847, 2021.
- [36] Muzammal Naseer, Kanchana Ranasinghe, Salman Khan, Fahad Shahbaz Khan, and Fatih Porikli. On improving adversarial transferability of vision transformers. *arXiv preprint arXiv:2106.04169*, 2021.
- [37] Kris Nicholson. Gpu based algorithms for terrain texturing. Master’s thesis, University of Canterbury, Christchurch, New Zealand, November 2008.
- [38] Joseph Redmon and Ali Farhadi. Yolov3: An incremental improvement. *arXiv preprint arXiv:1804.02767*, 2018.
- [39] Shaoqing Ren, Kaiming He, Ross Girshick, and Jian Sun. Faster r-cnn: Towards real-time object detection with region proposal networks. *Advances in Neural Information Processing Systems*, 28, 2015.
- [40] Dawn Song, Kevin Eykholt, Ivan Evtimov, Earlece Fernandes, Bo Li, Amir Rahmati, Florian Tramèr, Atul Prakash, and Tadayoshi Kohno. Physical adversarial examples for object detectors. In *12th USENIX workshop on offensive technologies (WOOT 18)*, 2018.
- [41] Naufal Suryanto, Yongsu Kim, Hyoeun Kang, Harashta Tatimma Larasati, Youngyeo Yun, Thi-Thu-Huong Le, Hunmin Yang, Se-Yoon Oh, and Howon Kim. Dta: Physical camouflage attacks using differentiable transformation network. In *Proceedings of the IEEE/CVF Conference on Computer Vision and Pattern Recognition*, pages 15305–15314, 2022.

- [42] Naufal Suryanto, Yongsu Kim, Harashta Tatimma Larasati, Hyoeun Kang, Thi-Thu-Huong Le, Yoonyoung Hong, Hunmin Yang, Se-Yoon Oh, and Howon Kim. Active: Towards highly transferable 3d physical camouflage for universal and robust vehicle evasion. In *Proceedings of the IEEE/CVF International Conference on Computer Vision*, pages 4305–4314, 2023.
- [43] Jia Tan, Nan Ji, Haidong Xie, and Xueshuang Xiang. Legitimate adversarial patches: Evading human eyes and detection models in the physical world. In *Proceedings of the 29th ACM International Conference on Multimedia*, pages 5307–5315, 2021.
- [44] Zhixian Tang, Kun Chen, Mingyuan Pan, Manning Wang, and Zhijian Song. An augmentation strategy for medical image processing based on statistical shape model and 3d thin plate spline for deep learning. *IEEE Access*, 7:133111–133121, 2019.
- [45] Simen Thys, Wiebe Van Ranst, and Toon Goedemé. Fooling automated surveillance cameras: adversarial patches to attack person detection. In *Proceedings of the IEEE/CVF Conference on Computer Vision and Pattern Recognition workshops*, pages 0–0, 2019.
- [46] Chien-Yao Wang, Alexey Bochkovskiy, and Hong-Yuan Mark Liao. Yolov7: Trainable bag-of-freebies sets new state-of-the-art for real-time object detectors. In *Proceedings of the IEEE/CVF Conference on Computer Vision and Pattern Recognition*, pages 7464–7475, 2023.
- [47] Donghua Wang, Tingsong Jiang, Jialiang Sun, Weien Zhou, Zhiqiang Gong, Xiaoya Zhang, Wen Yao, and Xiaoqian Chen. Fca: Learning a 3d full-coverage vehicle camouflage for multi-view physical adversarial attack. In *Proceedings of the AAAI Conference on Artificial Intelligence*, volume 36(2), pages 2414–2422, 2022.
- [48] Jiakai Wang, Aishan Liu, Zixin Yin, Shunchang Liu, Shiyu Tang, and Xianglong Liu. Dual attention suppression attack: Generate adversarial camouflage in physical world. In *Proceedings of the IEEE/CVF Conference on Computer Vision and Pattern Recognition*, pages 8565–8574, 2021.
- [49] Yi Wang, Jingyang Zhou, Tianlong Chen, Sijia Liu, Shiyu Chang, Chandrajit Bajaj, and Zhangyang Wang. Can 3d adversarial logos cloak humans? *arXiv preprint arXiv:2006.14655*, 2020.
- [50] Zhou Wang, Alan C Bovik, Hamid R Sheikh, and Eero P Simoncelli. Image quality assessment: from error visibility to structural similarity. *IEEE Transactions on Image Processing*, 13(4):600–612, 2004.
- [51] Jamie Watson, Michael Firman, Gabriel J Brostow, and Daniyar Turmukhambetov. Self-supervised monocular depth hints. In *Proceedings of the IEEE/CVF International Conference on Computer Vision*, pages 2162–2171, 2019.
- [52] Jamie Watson, Oisín Mac Aodha, Victor Prisacariu, Gabriel Brostow, and Michael Firman. The temporal opportunist: Self-supervised multi-frame monocular depth. In *Proceedings of the IEEE/CVF Conference on Computer Vision and Pattern Recognition*, pages 1164–1174, 2021.
- [53] Tong Wu, Xuefei Ning, Wenshuo Li, Ranran Huang, Huazhong Yang, and Yu Wang. Physical adversarial attack on vehicle detector in the carla simulator. *arXiv preprint arXiv:2007.16118*, 2020.
- [54] Zuxuan Wu, Ser-Nam Lim, Larry S Davis, and Tom Goldstein. Making an invisibility cloak: Real world adversarial attacks on object detectors. In *Computer Vision–ECCV 2020: 16th European Conference, Glasgow, UK, August 23–28, 2020, Proceedings, Part IV 16*, pages 1–17. Springer, 2020.
- [55] Zihao Xiao, Xianfeng Gao, Chilin Fu, Yinpeng Dong, Wei Gao, Xiaolu Zhang, Jun Zhou, and Jun Zhu. Improving transferability of adversarial patches on face recognition with generative models. In *Proceedings of the IEEE/CVF Conference on Computer Vision and Pattern Recognition*, pages 11845–11854, 2021.
- [56] Kaidi Xu, Gaoyuan Zhang, Sijia Liu, Quanfu Fan, Mengshu Sun, Hongge Chen, Pin-Yu Chen, Yanzhi Wang, and Xue Lin. Adversarial t-shirt! evading person detectors in a physical world. In *Computer Vision–ECCV 2020: 16th European Conference, Glasgow, UK, August 23–28, 2020, Proceedings, Part V 16*, pages 665–681. Springer, 2020.
- [57] Yang Zhang, Hassan Foroosh, Philip David, and Boqing Gong. Camou: Learning physical vehicle camouflages to adversarially attack detectors in the wild. In *International Conference on Learning Representations*, 2018.
- [58] Yang Zhang, PD Hassan Foroosh, and Boqing Gong. Camou: Learning a vehicle camouflage for physical adversarial attack on object detections in the wild. *International Conference on Learning Representation*, 2019.
- [59] Yiqi Zhong, Xianming Liu, Deming Zhai, Junjun Jiang, and Xiangyang Ji. Shadows can be dangerous: Stealthy and effective physical-world adversarial attack by natural phenomenon. In *Proceedings of the IEEE/CVF Conference on Computer Vision and Pattern Recognition*, pages 15345–15354, 2022.

- [60] Alon Zolfi, Shai Avidan, Yuval Elovici, and Asaf Shabtai. Adversarial mask: Real-world universal adversarial attack on face recognition models. In *Joint European Conference on Machine Learning and Knowledge Discovery in Databases*, pages 304–320. Springer, 2022.
- [61] Zhengxia Zou, Keyan Chen, Zhenwei Shi, Yuhong Guo, and Jieping Ye. Object detection in 20 years: A survey. *Proceedings of the IEEE*, 2023.